01 Sep 2014

Geophysical Signatures of Disseminated Iron Minerals: A Proxy for Understanding Subsurface Biophysicochemical Processes

Gamal Z. Abdel Aal

Estella A. Atekwana
Missouri University of Science and Technology, atekwana@mst.edu

Andre Revil

Recommended Citation

G. Z. Abdel Aal et al., "Geophysical Signatures of Disseminated Iron Minerals: A Proxy for Understanding Subsurface Biophysicochemical Processes," *Journal of Geophysical Research: Biogeosciences*, vol. 119, no. 9, pp. 1831-1849, American Geophysical Union (AGU), Sep 2014.
The definitive version is available at https://doi.org/10.1002/2014JG002659

AGU PUBLICATIONS

JGR

Journal of Geophysical Research: Biogeosciences

RESEARCH ARTICLE
10.1002/2014JG002659

Key Points:
- Iron minerals displayed different electrical and magnetic signatures
- Geophysical signatures are proxy for biophysicochemical processes
- Geophysical signatures can locate the marine sulfate-methane interface

Correspondence to:
G. Z. Abdel Aal,
gamal.abdel_aal@okstate.edu

Citation:
Abdel Aal, G. Z., E. A. Atekwana, and A. Revil (2014), Geophysical signatures of disseminated iron minerals: A proxy for understanding subsurface biophysicochemical processes, *J. Geophys. Res. Biogeosci.*, *119*, 1831–1849, doi:10.1002/2014JG002659.

Received 3 MAR 2014
Accepted 4 AUG 2014
Accepted article online 11 AUG 2014
Published online 18 SEP 2014

Geophysical signatures of disseminated iron minerals: A proxy for understanding subsurface biophysicochemical processes

Gamal Z. Abdel Aal[1,2], Estella A. Atekwana[1], and A. Revil[3,4]

[1]Boone Pickens School of Geology, Oklahoma State University, Stillwater, Oklahoma, USA, [2]Geology Department, Faculty of Science, Assiut University, Assiut, Egypt, [3]Colorado School of Mines, Department of Geophysics, Golden, Colorado, USA, [4]ISTerre, CNRS, UMR CNRS 5275, Université de Savoie, Chambéry, France

Abstract Previous studies have linked biogeophysical signatures to the presence of iron minerals resulting from distinct biophysicochemical processes. Utilizing geophysical methods as a proxy of such biophysicochemical processes requires an understanding of the geophysical signature of the different iron minerals. Laboratory experiments were conducted to investigate the complex conductivity and magnetic susceptibility signatures of five iron minerals disseminated in saturated porous media under variable iron mineral content and grain size. Both pyrite and magnetite show high quadrature and inphase conductivities compared to hematite, goethite, and siderite, whereas magnetite was the highly magnetic mineral dominating the magnetic susceptibility measurements. The quadrature conductivity spectra of both pyrite and magnetite exhibit a well-defined characteristic relaxation peak below 10 kHz, not observed with the other iron minerals. The quadrature conductivity and magnetic susceptibility of individual and a mixture of iron minerals are dominated and linearly proportional to the mass fraction of the highly conductive (pyrite and magnetite) and magnetic (magnetite) iron minerals, respectively. The quadrature conductivity magnitude increased with decreasing grain size diameter of magnetite and pyrite with a progressive shift of the characteristic relaxation peak toward higher frequencies. The quadrature conductivity response of a mixture of different grain sizes of iron minerals is shown to be additive, whereas magnetic susceptibility measurements were insensitive to the variation in grain size diameters (1–0.075 mm). The integration of complex conductivity and magnetic susceptibility measurements can therefore provide a complimentary tool for the successful investigation of in situ biophysicochemical processes resulting in biotransformation or secondary iron mineral precipitation.

1. Introduction

Microbial mineral interactions and biophysicochemical processes play an important role in the cycling of elements in the Earth and the coupling of many biogeochemical cycles. Most important are the linkages of carbon, sulfur, and iron biogeochemical cycles often resulting in the precipitation of a variety of minerals [*Lovley*, 1991, 1993; *Nealson and Saffarini*, 1994; *Kappler and Straub*, 2005; *Cooper et al.*, 2006; *Blöthe and Roden*, 2009]. Microbially mediated iron minerals are of particular significance because they comprise approximately 40% of all minerals formed by microorganisms [*Lowenstam*, 1986; *Bazylinski and Frankel*, 2003]. Many species of microorganisms, mainly anaerobic bacteria, are capable of reducing crystalline and amorphous Fe(III) oxides [*Lovley*, 1993; *Roden and Zachara*, 1996; *Zhang et al.*, 1997, 1998; *Roh et al.*, 2001]. Anaerobic Fe(III)-reducing bacteria precipitate or transform these iron oxides/hydroxides into crystalline Fe(II) containing mineral phases such as magnetite (Fe_3O_4), siderite ($FeCO_3$), vivianite [$Fe_3(PO_4) \cdot 2H_2O$], and iron sulfide (FeS) [*Postma*, 1981; *Zhang et al.*, 1997, 1998; *Fredrickson et al.*, 1998]. The presence of these biogenic Fe minerals may serve as physical indicators for previous biological activities in modern and ancient geological settings [*Liu et al.*, 1997; *Zhang et al.*, 1997, 1998] and may be used to infer either ongoing or past redox processes. Therefore, the development of techniques that are sensitive to the iron mineralogy, which are linked to different subsurface biogeochemical compartments, is sorely needed.

Compared with conventional borehole sampling and laboratory analysis, near-surface geophysical techniques provide such a potential. In particular, both induced polarization (IP) (or complex conductivity) and magnetic susceptibility methods are emerging techniques used for investigating abiotic and biotic processes resulting in iron mineral formation. The IP method has been applied to the study of metal-sand mixtures [*Gurin et al.*, 2013; *Mansoor and Slater*, 2007; *Slater et al.*, 2005, 2006; *Wu et al.*, 2005], monitoring of

biotic [*Flores Orozco et al*., 2011; *Ntarlagiannis et al*., 2005; *Williams et al*., 2005, 2009; *Slater*, 2007; *Personna et al*., 2008] and abiotic sulfide precipitation [*Ntarlagiannis et al*., 2010]. More recently, the magnetic susceptibility method has been used to map magnetic iron biominerals at hydrocarbon contaminated sites where iron reduction is coupled with the oxidation of organic carbon [*Rijal et al*., 2010, 2012; *Mewafy et al*., 2011, 2013; *Atekwana et al*., 2014]. In addition, laboratory studies have documented changes in magnetization associated with microbial precipitation of magnetite [*Porsch et al*., 2013; *Klueglein et al*., 2013]. Magnetic susceptibility measurements have also been used to map the sulfate-methane transition zone in marine sediments associated with anaerobic oxidation of methane where the diagenetic dissolution of primarily ferrimagnetic (titano)magnetite iron oxides around the iron redox boundary is occurring resulting in the total loss of magnetization and a distinct minima in the magnetic susceptibility [*Garming et al*., 2005; *Riedinger et al*., 2005].

In previous studies, the geophysical responses of the iron minerals are limited to the use of either complex conductivity or magnetic susceptibility which in turn is limited to the sensitivity of each method to the physical property of interest and may induce some ambiguity in the interpretation of the measured geophysical parameters. For example, some iron biominerals are conductive but less magnetic (e.g., pyrite) and therefore using only magnetic susceptibility measurements will not be successful in delineating the iron biomineral and the associated biogeochemical process (e.g., the delineation of sulfate reducing zones). In addition, to the best of our knowledge, there is no single study that has investigated the geophysical response of the mixture of different iron minerals or different grain sizes to mimic true complex subsurface conditions. Moreover, biotic laboratory experiments do not record the true geophysical responses of the biotic formed iron minerals since the interpretation of the results is complicated by the coupling of other biological (e.g., microbial growth and biofilm development) and geochemical (e.g., changes in fluid chemistry due to metabolic byproducts) changes [*Revil et al*., 2012a]. Therefore, integrating both complex conductivity and magnetic susceptibility techniques will have the potential of minimizing the ambiguity in the interpretation of the geophysical response (resulting from using only one technique) as well as recording the true geophysical signatures of these iron phase minerals.

In this work, we report on the results of several abiotic laboratory experiments conducted under fully saturated conditions to investigate the complex conductivity and magnetic susceptibility signatures of (i) different iron mineral phases (pyrite, magnetite, goethite, hematite, and siderite), (ii) mixtures of equal proportions of iron minerals, and (iii) different iron mineral mass content and grain size. Our results suggest that geophysical methods can be used as complementary tools for the monitoring of biophysicochemical processes resulting in different iron mineral phase formation with implications for iron biomineralization and iron cycling studies.

2. Complex Conductivity

Complex conductivity (or induced polarization) is an extension of the classical electrical resistivity method broadly used in hydrogeophysics (see a recent review of both methods in *Revil et al*. [2012b]). In complex conductivity, we consider both the magnitude and phase lag between the electrical field and the current density in a broad frequency range, typically going from 1 mHz to few tens of kHz (100 Hz in field conditions). The measured frequency-dependent complex conductivity σ^* (ω) of a porous medium can be represented with an inphase (real) conductivity component (σ') or electromigration term, and a quadrature (quadrature) conductivity component (σ'') or polarization term. The inphase and quadrature conductivities can be calculated from the measured impedance magnitude $|\sigma|$ and the phase shift φ of the sample as follows:

$$\sigma' = |\sigma| \cos\varphi, \tag{1}$$

$$\sigma'' = |\sigma| \sin\varphi. \tag{2}$$

The inphase (real, σ') conductivity component represents ohmic conduction currents that contain a bulk conductivity in the pore water and a surface conductivity [*Waxman and Smits*, 1968; *Lesmes and Frye*, 2001]. The surface conductivity results from surface conduction via the formation of an electrical double layer (EDL) at the grain-fluid interface [*Revil and Glover*, 1998]. The out of phase (quadrature or quadrature) conductivity σ'' represents the polarization term associated with the reversible storage of electrical charges in porous media. At low frequencies ($<$1 kHz), this contribution can be modeled as a function of the physicochemical

properties of the grain-fluid interface [*Vinegar and Waxman*, 1984; *Dukhin and Shilov*, 2002; *Vaudelet et al*., 2011a, 2011b]. Conduction and polarization of the electrical double layer is a function of specific surface area, surface charge density, surface ionic mobility, and bulk tortuosity [*Schön*, 1996; *Revil and Glover*, 1998; *Lesmes and Frye*, 2001; *Revil et al*., 2013].

At low frequencies (<1 kHz), several conduction and polarization mechanisms can exist in saturated iron mineral containing sediments [*Wu et al*., 2005, 2009]. A complex interfacial conductivity (σ^*_{int}) represents conduction and polarization processes occurring at the iron mineral/electrolyte interface, whereas an electronic conduction term accounts for conduction via interconnected electronically conductive iron minerals. The complex conductivity of the metallic particles incorporates both conduction and polarization within the electrical double layer (EDL) occurring at the electrolyte/iron mineral interface which includes a diffusive mechanism associated with ion migration to and from the metallic surface [*Wong*, 1979; *Slater et al*., 2005] and an electrochemical mechanism associated with redox active ions that transfer electrons across the mineral/electrolyte interface, via redox reactions, to the particle that can be an electronic conductor or a semiconductor [*Wong*, 1979]. Whereas the measured in phase depends on electrolytic conduction, electronic conduction, and interfacial conduction, the quadrature conductivity is only dependent on the interfacial properties of iron minerals. Also, the interfacial conduction appears to depend on the surface area of the iron mineral particles in porous media [*Slater et al*., 2005, 2006].

3. Magnetic Susceptibility

Magnetic susceptibility measurements are a nondestructive and cost effective method of determining the presence of iron-bearing minerals within the sediments. The magnetic susceptibility of a mineral or sediment is the physical quantity reflecting the ease with which that mineral or sediment can become magnetized when placed in a magnetic field [*Marcon et al*., 2011]. Magnetic susceptibility is defined as the ratio between magnetization, **M**, of the material in the magnetic field and the field intensity, **H** [*Mullins*, 1977; *Dearing et al*., 1985]:

$$\mathbf{M} = \chi_b \mathbf{H} \tag{3}$$

where χ_b denotes the bulk magnetic susceptibility of the material. Because **M** and **H** have the same units (A/m), χ_b is dimensionless. In practice, the magnetic response of a substance to an applied field can be normalized by volume or by mass or not normalized at all. The volume susceptibility, χ_v, is dimensionless in SI units, whereas the mass susceptibility, χ_m, is measured in m^3/kg. The magnetic susceptibility of unconsolidated sediments varies according to the type, volume fraction, size, and shape of the magnetic minerals disseminated in the sediments [*Mullins*, 1977]. All materials can be classified by the value of their magnetic susceptibility into three major groups: diamagnetic materials ($-1 < \chi_b < 0$), paramagnetic materials ($0 < \chi_b \leq 1$), and ferromagnetic materials ($\chi_b \geq 1$). Although all minerals exhibit some degree of magnetic behavior, ferrimagnetism is the most important among magnetic minerals in soils and sediments [*Dearing et al*., 1985]. Ferrimagnetism results from the unique alignment of the magnetic moments within minerals such as magnetite.

4. Materials and Methods

4.1. Iron Minerals Preparation

Five different iron minerals were selected for the present study which represents iron oxides (magnetite Fe_3O_4 and hematite α-Fe_2O_3), iron oxyhydroxides (goethite α-FeO (OH)), iron sulfides (pyrite FeS_2), and iron carbonates (siderite $FeCO_3$). The iron mineral specimens were obtained from the Geology Department at Oklahoma State University with purity up to 99%. The specimens were crushed into fine particles using a rock crusher and sieved into different grain size diameters (1–0.6, 0.6–0.3, 0.3–0.15, 0.15–0.075, and <0.075 mm). The sieved iron minerals were immediately stored in air tight closed container to avoid possible oxidation due to long exposure to air and for later use for the different experiments.

4.2. Porous Medium and Pore Fluid

The porous medium used for the experiments consisted of fine silica Ottawa sands (U.S. Silica Company) with a median grain diameter distribution $d_{50} = 200 \pm 10$ μm and a porosity of 0.45 ± 0.02 (calculated from the total

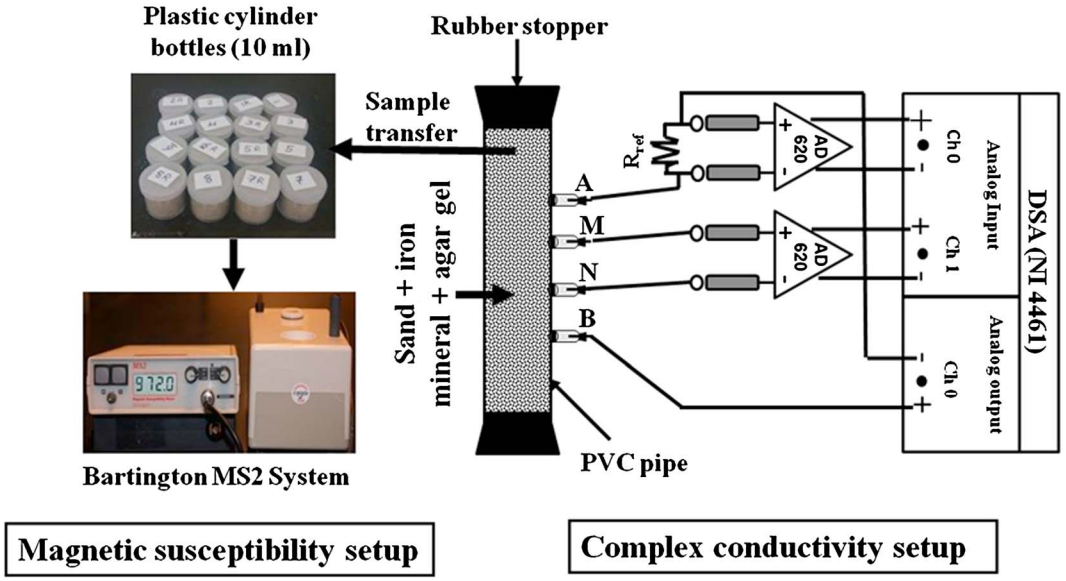

Figure 1. Schematic of column setup and instrumentation used in complex conductivity and magnetic susceptibility measurements. The complex conductivity measurements are obtained using a dynamic signal analyzer (DSA) (National Instruments (NIs)–4461) and AD620 preamplifier to boost the input impedance on the voltage channel and prevented current leakage into the circuitry (the system sensitivity is less than 0.1 mrad at frequencies below 100 Hz). The magnetic susceptibility measurements are obtained with BartingtonMS2 magnetic susceptibility meter and MS2B dual frequency sensor (operating frequency 4.65 kHz ±1% and maximum resolution of 2×10^{-6} SI).

volume of the column minus the volume of the dry sand). The fluid used to saturate the sand was agar gel, which is chosen to provide a homogenous distribution of the disseminated iron mineral particles when mixed with sand. Also, the agar gel prevented the settling of the iron mineral particles to the base of the sample holder due to the high density of these minerals. The Agar gel was prepared by dissolving 10 g of agar (BD Difco) into 1000 mL of DIW under stirring and heating up to 70°C. After cooling, the agar gel has an electrical conductivity of 0.0256 ± 0.003 S/m and a pH of 6.13 ± 0.01. In addition, sodium chloride (NaCl) solution with the same conductivity and pH of agar gel was prepared.

4.3. Sample Holder and Instrumentation Setup

A schematic representation of the complex conductivity and magnetic susceptibility setup used in this study is shown in Figure 1. For the complex conductivity measurements, the sample holder/column was constructed from polyvinyl chloride (PVC) pipe with an inner diameter of 3.4 cm and a length of 12 cm. Four nonpolarizing Ag-AgCl electrodes housed in electrolyte (agar gel mixed in 3 M concentration of KCl) filled chambers were placed 2 cm apart along the length of the column and located just outside the current flow path. The outer two electrodes were used to inject the current sinusoid, and the two inner electrodes were used to record the output voltage sinusoid. Two rubber stoppers were used to cap the two ends of the column after packing with the mixture of iron, agar gel, and sand. The four nonpolarizable electrodes (AB for the current and MN for the voltage) were connected to a dynamic signal analyzer (DSA) (National Instruments (NIs)–4461) to perform the complex conductivity measurements between 0.1 Hz and 10 kHz at 16 equal logarithmic intervals (sensitivity of 0.1 mrad over this frequency range). An AD620 preamplifier boosted the input impedance on the voltage channel and prevented current leakage into the circuitry. The impedance magnitude $|\sigma|$ and the phase shift φ (between a measured voltage sinusoid and an impressed current sinusoid) of the sample were measured relative to a high-quality resistor. The real (σ') and quadrature (σ'') parts of the sample complex conductivity (equations (1) and (2)) were then calculated. After the complex conductivity measurements, three samples were retrieved and transferred from the sand column into 10 mL cylindrical plastic bottles. Then the volumetric magnetic susceptibility (χ_v) measurements were obtained using a Bartington MS2 magnetic susceptibility meter and MS2B dual frequency sensor (operating frequency 4.65 kHz ±1% and maximum resolution of 2×10^{-6} SI for χ_v).

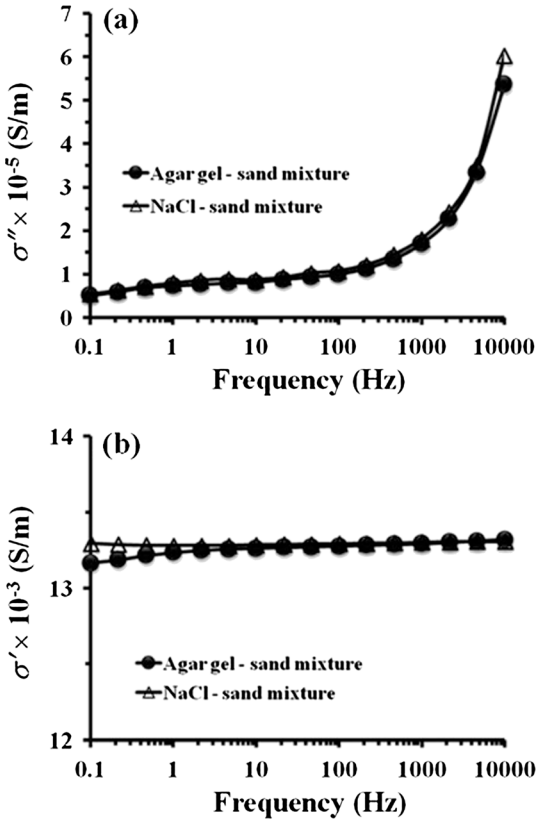

Figure 2. Results of complex conductivity measurements, (a) quadrature conductivity (σ'') and (b) inphase conductivity (σ') of agar gel-sand mixture and NaCl-sand mixture with electrolytic conductivity of 0.0256 ± 0.003 S/m. There is a minimal difference between the complex conductivity response of agar gel-sand mixture and NaCl-sand mixture.

5. Experimental Procedure

5.1. Complex Conductivity

Two control experiments were conducted to investigate (1) the effect of agar gel viscosity on the measured complex conductivity response by comparing the complex conductivity response of agar gel-sand mixture versus NaCl-sand mixture with the same electrolytic conductivity (0.0256 ± 0.003 S/m) and (2) the effect of packing and the reproducibility of complex conductivity response by conducting triplicate complex conductivity measurements of agar gel-sand mixture. Following these control experiments, five main laboratory experiments (I–VI) were conducted with the prepared different iron mineral phases using complex conductivity measurements in saturated sand columns. All experiments are conducted at the same ambient laboratory temperature, typically 22 ± 1°C. The same procedure was applied to all the experiments by mixing one pore volume of agar gel to fixed amount (250 g) of fine sands and the experimentally iron minerals under different conditions. The agar gel-fine sand-iron mineral mixture was packed into the constructed PVC pipe, and complex conductivity measurements were obtained in the frequency range of 0.1 Hz–10 kHz. Experiment (I) was conducted to investigate the complex conductivity response of each of the five iron phase minerals (pyrite, magnetite, goethite, hematite, and siderite) with the same content (1% w/w or 10 $mg_{iron\ mineral}/g_{sand}$) and grain diameter (0.3–0.15 mm).

In experiment (II), four different iron mineral mixtures (magnetite + hematite, magnetite + goethite, magnetite + siderite, and magnetite + pyrite) were prepared with equal proportions (1% w/w or 10 $mg_{iron\ mineral}/g_{sand}$ of each using the same grain diameter of 0.3–0.15 mm) and complex conductivity measurements were obtained. Experiment (III) was performed to investigate the effect of different iron mineral content (0, 1.5, 5, 10, and 20 $mg_{iron\ mineral}/g_{sand}$) with fixed grain diameter (0.3–0.15 mm) in the complex conductivity response of saturated fine sand. The experiment was conducted using magnetite and pyrite as examples as they have been the focus of many recent laboratory and field biogeophysical studies. Experiment (IV) was performed to investigate the effect of different grain diameters of magnetite and pyrite using the following range of sizes: 1–0.6, 0.6–0.3, 0.3–0.15, 0.15–0.075, and <0.075 mm. This experiment was conducted with fixed iron mineral content of 1% (10 $mg_{iron\ mineral}/g_{sand}$) and varying the iron grain size diameter of magnetite or pyrite from 1–0.6 mm to <0.075 mm. To further investigate the effect of grain size diameters of iron minerals, three mixtures of equal proportions (0.5% w/w or 5 mg_{pyrite}/g_{sand}) of different grain size diameters of pyrite (<0.075 mm + 1–0.6 mm, 0.3–0.6 mm + 1–0.6 mm, and <0.075 mm + 0.3–0.15 mm) were prepared and complex conductivity measurements were obtained (experiment V).

5.2. Magnetic Susceptibility

The magnetic susceptibility measurements were performed by retrieving three samples from the sand columns (top, middle, and bottom) after each experiment with the complex conductivity measurements. The samples were transferred into 10 mL cylindrical plastic bottles, and volumetric magnetic susceptibility measurements were obtained. The error associated with three measurements relative to the average values

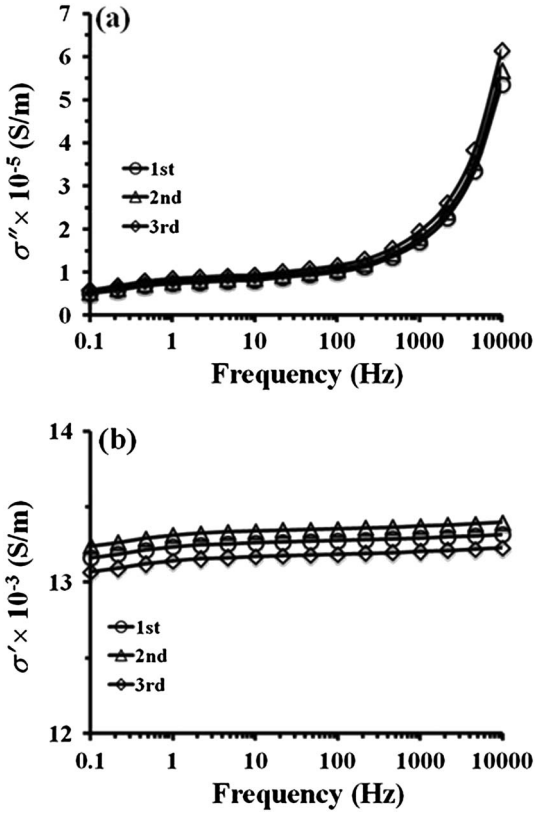

Figure 3. Results of complex conductivity measurements, (a) quadrature conductivity (σ'') and (b) inphase conductivity (σ') of triplicate agar gel-sand mixture (background) packed three times show very good reproducibility of the triplicate complex conductivity response of the agar gel-sand mixture.

was determined using the standard deviation calculation. The first set of measurements was conducted in samples containing individual iron mineral phases (10 $mg_{iron\ mineral}/g_{sand}$ and grain diameter of 3–0.15 mm). The second set of measurements were conducted for the four different iron minerals mixtures (magnetite + hematite, magnetite + goethite, magnetite + siderite, and magnetite + pyrite) with equal proportions (1% w/w or 10 $mg_{iron\ mineral}/g_{sand}$ of each using the same grain diameter of 0.3–0.15 mm) as well as a mixture of equal proportions of the five iron minerals (magnetite + pyrite + hematite + goethite + siderite). For the third experiment, magnetic susceptibility measurements were obtained on samples with different magnetite content (0, 1.5, 5, 10, and 20 $mg_{magnetite}/g_{sand}$) with a grain diameter of 0.3–0.15 mm. The final set of magnetic susceptibility measurements were conducted on samples with varying grain size diameters (1–0.6, 0.6–0.3, 0.3–0.15, 0.15–0.075, and $<$0.075 mm) of magnetite mineral (10 $mg_{magnetite}/g_{sand}$).

6. Results

6.1. Complex Conductivity Results

6.1.1. Control Experiments

The quadrature conductivity (σ'') component (Figure 2a) and the inphase conductivity component (σ') (Figure 2b) of both agar gel-sand mixture and NaCl-sand mixture are relatively the same. The quadrature conductivity (σ'') magnitude of the NaCl-sand mixture shows a 2.3% change from the agar gel-sand mixture at 0.1 Hz, which increases to 5.6% change 10,000 Hz (Figure 2a). Similarly, the inphase conductivity component (σ') of NaCl-sand mixture shows a percent change from the agar gel-sand mixture of 0.1 at 0.1 Hz, increases to 1 at 10,000 Hz (Figure 2b). These results indicate that the viscosity of the agar gel has minimal effect on the measured complex conductivity response.

The calculated standard deviations from the average of the triplicate measured quadrature conductivity (σ'') component (Figure 3a) and the inphase conductivity (σ') component (Figure 3b) of the agar gel-sand mixture with the same conditions range from 0.03 to 0.33×10^{-5} S/m and 0.0.70 to 0.069×10^{-3} S/m, respectively. These results show that the sample packing has minimal effect as the complex conductivity response is highly reproducible within the frequency range of 0.1–10,000 Hz.

6.1.2. Signature of Iron Minerals

At frequencies below 1 Hz, the magnitude of the quadrature conductivity (σ'') component displays small variation between all measured iron minerals and the background clean sand (no iron minerals) with an average value of $0.52 \times 10^{-5} \pm 0.003 \times 10^{-5}$ S/m) (Figure 4a). At frequencies above 1 Hz, the measured iron minerals can be arranged based on the magnitude of the quadrature conductivity values as (pyrite $>$ magnetite$>>$ hematite $>$ goethite $>$ siderite) with goethite and siderite showing quadrature conductivity response very close to the background clean sand (Figure 4a). However, disseminated hematite shows an increase in the quadrature conductivity magnitudes above 100 Hz exceeding the quadrature conductivity magnitudes of pyrite at a frequency of 10 kHz (Figure 4a). Both pyrite and

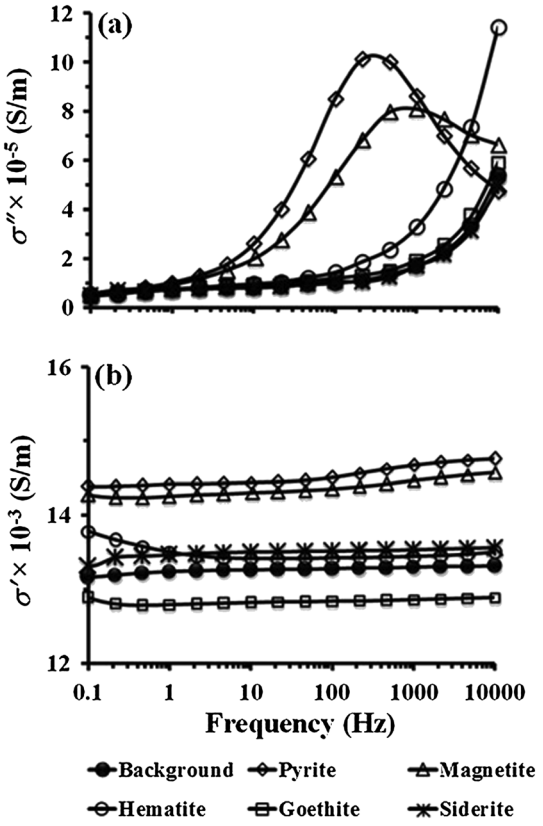

Figure 4. Results of complex conductivity measurements, (a) quadrature conductivity (σ'') and (b) inphase conductivity (σ') of different iron mineral phases (10 $mg_{iron\ mineral}/g_{sand}$ and grain diameter of 0.3–0.15 mm) disseminated in saturated fine sand. The different iron minerals show quadrature conductivity magnitudes in the order of pyrite > magnetite > hematite > goethite > siderite with insignificant changes in the inphase conductivity. Both pyrite and magnetite show a well-defined relaxation peak in the quadrature conductivity response below 1000 Hz, not observed with the other iron minerals.

magnetite show a well-defined relaxation peak in the σ'' spectra centered at frequencies of 250 Hz and 1000 Hz with quadrature conductivity magnitude of 10.01×10^{-5} S/m and 7.97×10^{-5} S/m, respectively (Figure 4a). These relaxation peaks in the quadrature conductivity spectra are not observed with the hematite, goethite, and siderite within the applied frequency range (0.1–10 kHz). The change in the magnitude of the inphase conductivity component (σ') of the measured iron minerals was low (around $13.61 \times 10^{-3} \pm 1.00$ S/m) compared to the quadrature conductivity (Figure 4b). The percent changes in the inphase conductivity magnitude of the iron minerals from the background are +8.92, +7.67, +1.98, +1.74, and −3.38 for pyrite, magnetite, hematite, siderite, and goethite, respectively (Figure 4b).

6.1.3. Signature of Mixed Iron Minerals

At frequencies above 1 Hz, the mixture of equal proportions of (magnetite + hematite), (magnetite + goethite), and (magnetite + siderite) show higher quadrature conductivity magnitude compared to the individual response of hematite, goethite, and siderite (Figures 5a–5c). The mixtures show about 10% decrease in the quadrature conductivity magnitude relative to the magnetite by itself which continue to decrease to about 15% at higher frequencies (10 kHz) except for the case of (magnetite + siderite) which increases by almost 1 order of magnitude (Figures 5a–5c). Moreover, the quadrature conductivity spectra of the mixtures are characterized by the presence of well-defined relaxation peaks centered at 1 kHz similar to the relaxation peak of the magnetite mineral (Figures 5a–5c). On the other hand, the mixture of equal proportions of (magnetite + pyrite) displays an increase in the quadrature conductivity magnitude by about 75% and 120% (at 500 Hz) relative to the individual pyrite and magnetite, respectively (Figure 5d). The quadrature conductivity response of the mixture of (magnetite + pyrite) displays a well-defined relaxation peak centered at 250 Hz similar to the relaxation peak of the pyrite mineral (Figure 5d).

The addition of equal proportions of magnetite to hematite, goethite, and siderite result in a decrease in the magnitude of the inphase conductivity response compared to the magnetite which is slightly lower than or equal to the individual inphase conductivity response of the hematite, goethite, and siderite minerals (Figures 6a–6c). However, the addition of equal proportions of magnetite to pyrite increases the magnitude of the inphase conductivity response by 4.7% and 5.7% compared to the individual inphase conductivity response of magnetite and pyrite, respectively (Figure 6d). Similar inphase and quadrature conductivity results were obtained (not shown here) for the mixture of pyrite with hematite, goethite, and siderite.

6.1.4. Effect of Iron Mineral Content

At frequencies above 1 Hz, the magnitude of the quadrature conductivity increases with increasing pyrite and magnetite content with the development of well-defined relaxation peaks centered at

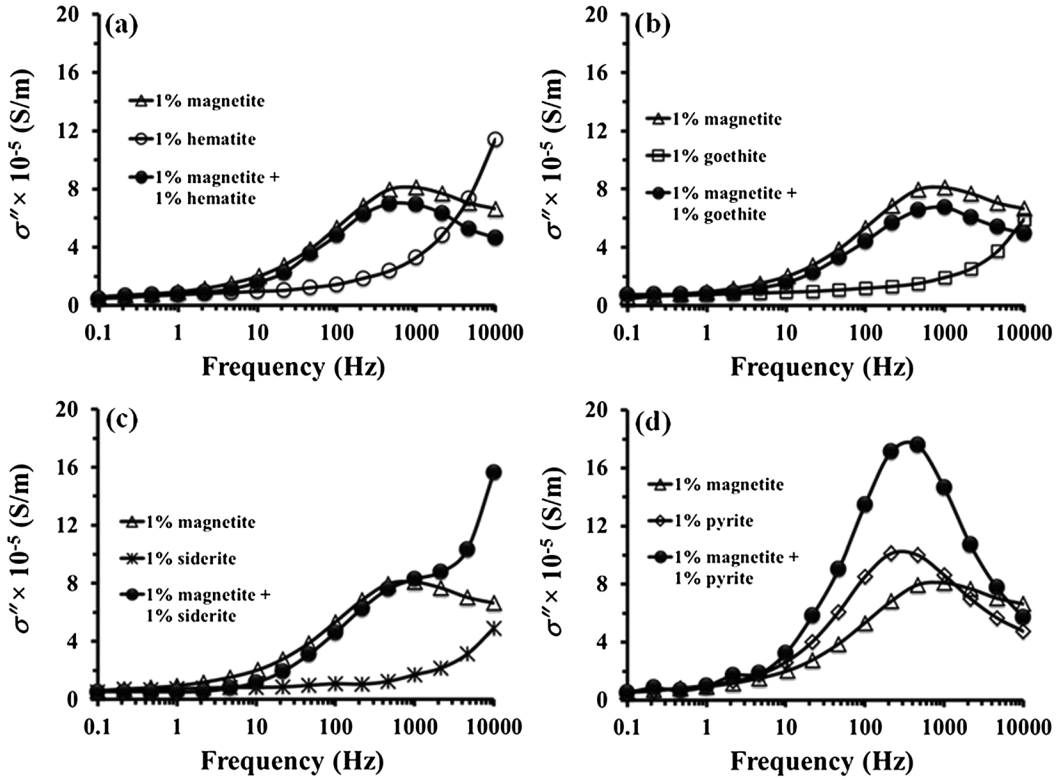

Figure 5. Quadrature conductivity (σ'') response as a function of frequency for 1% (10 $mg_{iron\ mineral}/g_{sand}$) of individual magnetite, pyrite, hematite, goethite, and siderite iron minerals (with open symbols) and mixtures of equal proportions (1:1 with 1% = 10 $mg_{iron\ mineral}/g_{sand}$) of different iron minerals (a) magnetite + hematite, (b) magnetite + goethite, (c) magnetite + siderite, and (c) magnetite + pyrite (filled symbols), disseminated in saturated fine sand. The grain diameters for each of the iron minerals were maintained to 0.3–0.15 mm. The mixtures of magnetite + hematite, magnetite + goethite, and magnetite + siderite show a decrease in the magnitude of quadrature conductivity except for the mixture of magnetite + pyrite.

1000 Hz and 250 Hz for magnetite and pyrite, respectively (Figures 7a and 7b). At lower magnetite and pyrite contents, the relaxation peaks are broader in shape and become narrower at higher content (Figures 7a and 7b). The increase in the magnitude of the quadrature conductivity with increasing iron mineral content was relatively higher in the case of pyrite compared to magnetite (Figures 7a–7c). At the relaxation frequencies, the quadrature conductivity magnitude of magnetite increases from 2.79×10^{-5} to 14.83×10^{-5} S/m and pyrite from 2.93×10^{-5} to 18.25×10^{-5} S/m by increasing the content of the disseminated minerals from 1.5 to 20 $mg_{iron\ mineral}/g_{sand}$, respectively (Figures 7a and 7b). Figure 7c shows that the relationship between the quadrature conductivity magnitude at the relaxation peaks and the content of magnetite and pyrite can be fitted with a power law relationship. The power law exponents of pyrite (0.68, obtained from $\sigma''\times10^{-5} = 2.24\times \text{pyrite}_{(mg/g\ sand)}^{0.68}$) and magnetite (0.64, obtained from $\sigma''\times10^{-5} = 1.97\times \text{magnetite}_{(mg/g\ sand)}^{0.64}$) are relatively equal indicating that the rate of change in the quadrature conductivity magnitude as a function of pyrite and magnetite are relatively the same as demonstrated by the power law relationships shown in Figure 7c.

The increase in magnetite and pyrite content shows relatively small change in the σ' response (with a percent change of 2.69 for magnetite and 13.37 for pyrite) compared to quadrature conductivity (with a percent change of 431.54 for magnetite and 491.77 for pyrite) (Figures 7d–7f). The inphase conductivity magnitude of magnetite displays minimal changes from the background with an average value of $13.19\pm0.03\times10^{-3}$ S/m, except at content of 10 $mg_{iron\ mineral}/g_{sand}$ which increases to 14.47×10^{-3} S/m (Figure 7d). The inphase conductivity magnitude of pyrite increases from 13.37×10^{-3} to 15.03×10^{-3} S/m by increasing the content from 1.5 to 20 $mg_{iron\ mineral}/g_{sand}$, respectively (Figure 7e). The established power law relationship of the inphase conductivity magnitude versus iron mineral content

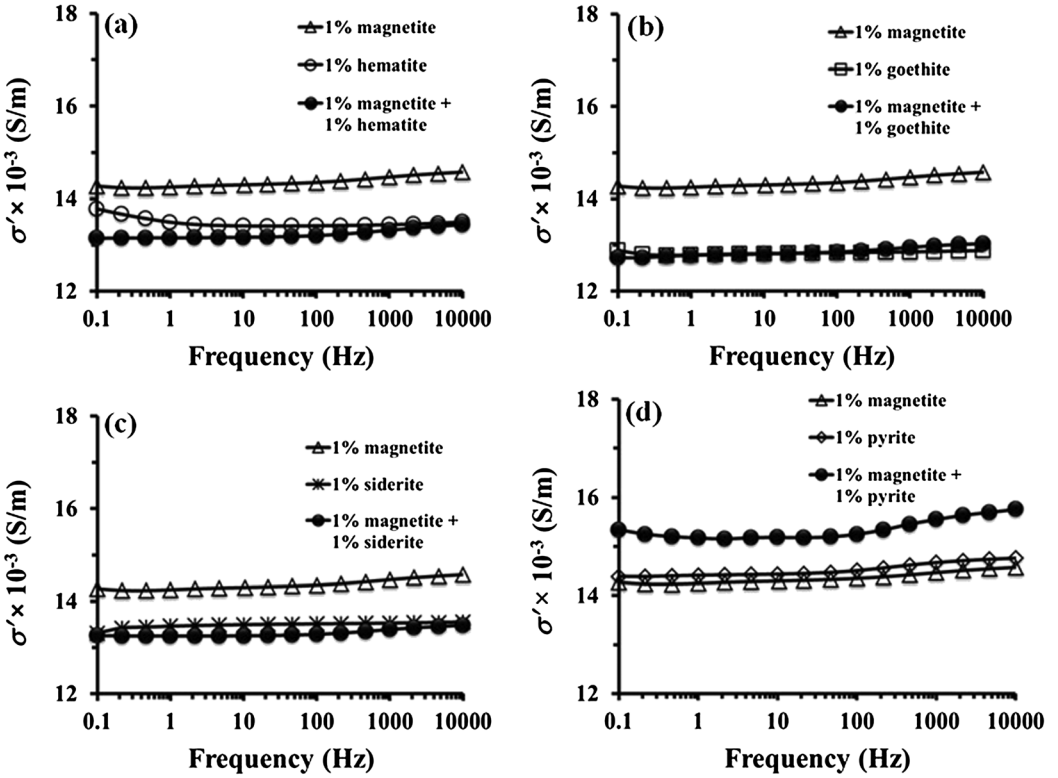

Figure 6. Inphase conductivity (σ') response as a function of frequency for 1% (10 $mg_{iron\ mineral}/g_{sand}$) of individual magnetite, pyrite, hematite, goethite, and siderite iron minerals (with open symbols) and mixtures of equal proportions (1:1 with 1% = 10 $mg_{iron\ mineral}/g_{sand}$) of different iron minerals (a) magnetite + hematite, (b) magnetite + goethite, (c) magnetite + siderite, and (c) magnetite + pyrite (filled symbols), disseminated in saturated fine sand. The grain diameters for each of the iron minerals were maintained to 0.3–0.15 mm. The mixtures of magnetite + hematite, magnetite + goethite, and magnetite + siderite show a decrease in the magnitude of inphase conductivity except for the mixture of magnetite + pyrite.

($\sigma' \times 10^{-3} = 13.13 \times \text{magnetite}_{\text{(mg/g sand)}}^{0.02}$ for magnetite and ($\sigma' \times 10^{-3} = 13.08 \times \text{pyrite}_{\text{(mg/g sand)}}^{0.05}$) shows that the power law exponent of magnetite (0.02) is smaller than for pyrite (0.05) with correlation coefficients (R^2) of 0.28 and 0.99 for magnetite and pyrite, respectively (Figure 7f).

6.1.5. Effect of Iron Mineral Grain Diameters

The quadrature conductivity magnitude increases, and characteristic relaxation peaks progressively shift toward higher frequencies with decreasing the grain size diameters (1–0.6, 0.6–0.3, 0.3–0.15, 0.15–0.075, to <0.075 mm) of the disseminated magnetite and pyrite (Figures 8a and 8b). The central frequencies of the relaxation peaks of the quadrature conductivity spectra of magnetite (250, 500, 1000, 2150, and 10,000 Hz) are higher than those of pyrite (50, 100, 250, 1000, and 10,000 Hz) (Figures 6a and 6b). At the relaxation frequencies, the quadrature conductivity magnitude of magnetite mineral increases from 5.52×10^{-5} to 20.71×10^{-5} S/m and pyrite mineral from 6.87×10^{-5} to 29.26×10^{-5} S/m by decreasing the grain size diameters of the disseminated minerals from 1–0.6 mm to <0.075 mm (Figures 8a and 8b). Figure 8c shows that the relationship between the σ'' magnitude at the relaxation peaks and the grain size diameters of magnetite and pyrite can be fitted with a power law relationship. At the relaxation frequencies, the σ'' magnitude of magnetite mineral is lower than pyrite; however, the power law exponents are relatively the same [0.50 for magnetite ($\sigma'' \times 10^{-5} = 5.09 \times \text{magnetite}_{\text{(grain diameter in mm)}}^{-0.50}$) and 0.51 for pyrite ($\sigma'' \times 10^{-5} = 6.48 \times \text{pyrite}_{\text{(grain diameter in mm)}}^{-0.51}$)] (Figure 8c).

The inphase conductivity of magnetite mineral increases from 14.58×10^{-3} to 15.58×10^{-3} S/m and pyrite mineral from 13.98×10^{-3} to 19.62×10^{-3} S/m by decreasing the grain size diameters of the disseminated minerals from 1–0.6 mm to <0.075 mm (Figures 8d and 8e). The increase in inphase

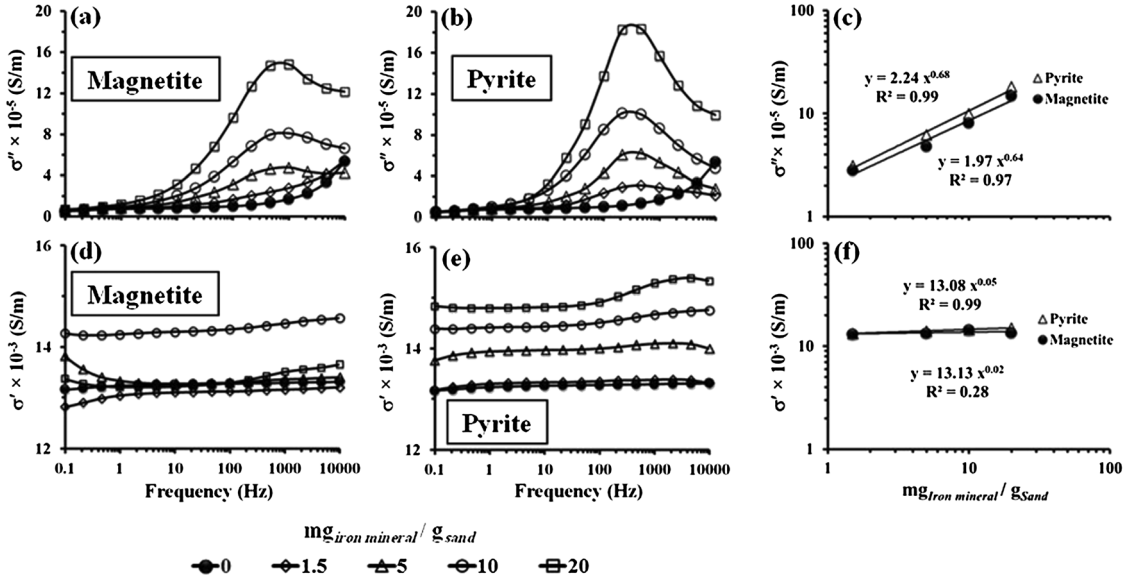

Figure 7. Results of complex conductivity measurements (σ'' and σ') of different mass content (0, 1.5, 5, 10, and 20 $mg_{iron\ mineral}/g_{sand}$) and fixed grain size diameter (0.3–0.15 mm) of (a and d) magnetite and (b and e) pyrite with (c and f) power law relationships of the complex conductivity measurements at the relaxation peaks versus mass content of the two iron minerals. The quadrature conductivity (σ'') magnitude increases with increasing the content of magnetite and pyrite with pyrite being the highest. The inphase conductivity (σ') magnitude shows insignificant change with increasing the content of magnetite and pyrite.

conductivity magnitude as a function of grain diameters is relatively smaller (with a percent change of 6.92 for magnetite and 40.27 for pyrite) than the quadrature conductivity (with a percent change of 275.31 for magnetite and 326.19 for pyrite) with pyrite being the highest (Figures 8d and 8f). The power law exponent of magnetite (0.04 obtained from $(\sigma' \times 10^{-3} = 13.84 \times \text{magnetite}_{\text{(grain diameter in mm)}}^{-0.04})$ is 3 times lower than pyrite (0.12 obtained from $(\sigma' \times 10^{-3} = 13.50 \times \text{pyrite}_{\text{(grain diameter in mm)}}^{-0.12})$ as

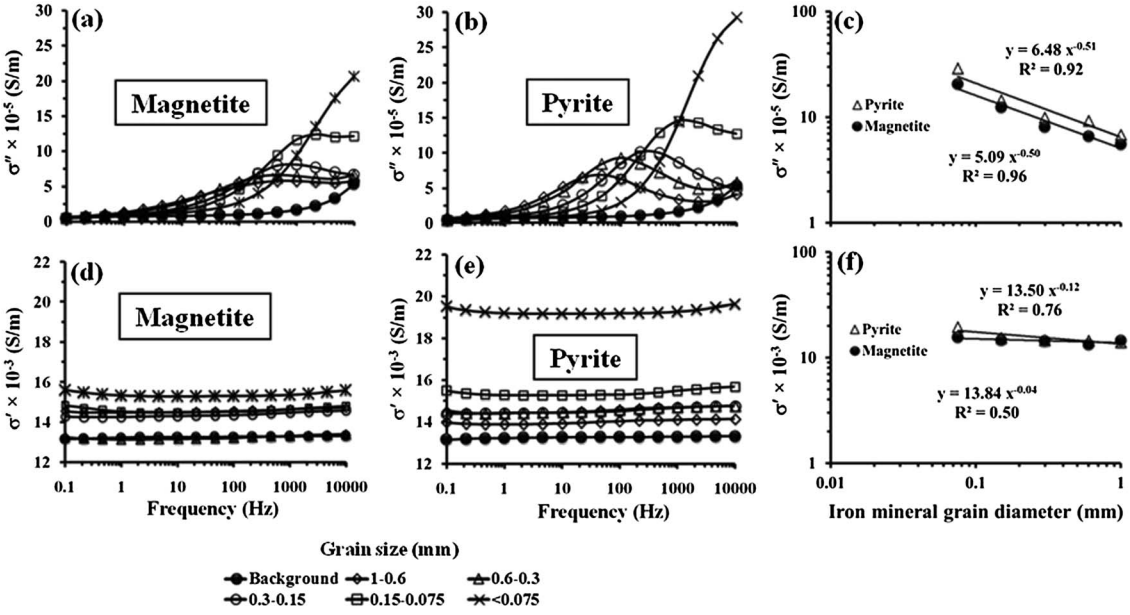

Figure 8. Results of complex conductivity measurements (σ'' and σ') of different grain size (1–0.6, 0.6–0.3, 0.3–0.15, 0.15–0.075, and <0.075 mm) and fixed content (10 $mg_{iron\ mineral}/g_{sand}$) of (a and d) magnetite and (b and e) pyrite with (c and f) power law relationships of the complex conductivity measurements at the relaxation peaks versus grain size diameters of the two iron minerals. The quadrature conductivity (σ'') magnitude increases with decreasing the grain size diameters of magnetite and pyrite with a progressive shift in relaxation peak into higher frequency. The quadrature conductivity of pyrite is higher than magnetite with insignificant change in the inphase conductivity (σ') magnitude.

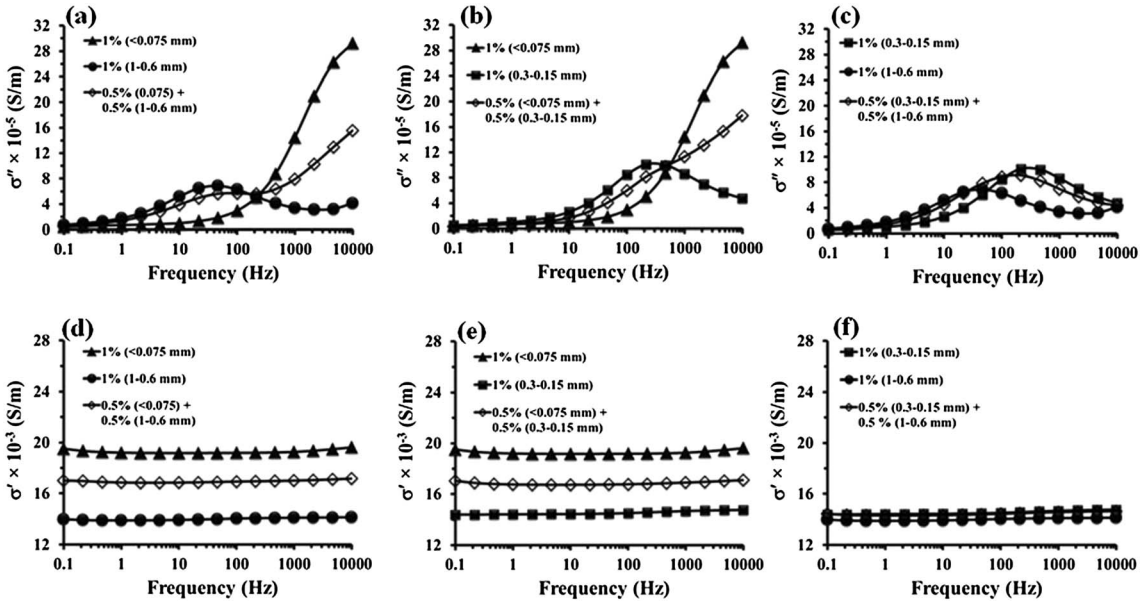

Figure 9. Results of (a–c) quadrature (σ'') (d–f) and inphase (σ') conductivity measurements of individual grain size diameters (1% = 10 mg_{pyrite}/g_{sand} of 1–0.6, 0.3–0.15, and <0.075 mm) and mixtures of equal proportions of grain size diameters (1:1 of 0.5% = 5 mg_{pyrite}/g_{sand} of <0.075 + 1–0.6 mm and <0.075 + 0.3–0.15) of pyrite disseminated in saturated fine sand. The quadrature (σ'') and inphase (σ') conductivity of the mixtures show additive response averaged between the two different grain size diameters.

shown from the established power law relationship of the σ' magnitude versus iron mineral grain diameter for magnetite and pyrite (Figure 8f).

6.1.6. Effect of Mixed Iron Minerals Grain Diameters

The magnitude of the quadrature conductivity and observed relaxation peaks of the mixtures of equal proportions of two different grain size diameters of pyrite show average values of quadrature conductivity magnitudes and relaxation peaks of the two individual grain size diameters (Figures 9a–9c). In other words, the quadrature conductivity magnitude and observed relaxation peaks of the mixtures of equal proportions of two different grain size diameters of pyrite are additive. Similarly, the inphase magnitudes of the mixtures of equal proportions of two different grain size diameters of pyrite display average values for the sum of the inphase magnitudes of the individual grain size diameters of pyrite (Figures 9d–9f). Furthermore, the individual and mixtures of the two different grain size diameters of pyrite display a wide range in inphase values (14×10^{-3} to 19×10^{-3} S/m) except for the mixture and individual grain diameters of 0.3–0.15 mm and 1–0.6 mm which display a very narrow range in in phase (14×10^{-3} to 14.4×10^{-3} S/m).

6.2. Magnetic Susceptibility

In general, the calculated standard deviation from the average of the triplicate measured sample was found to be less than 1.25 SI. The results of the volumetric magnetic susceptibility (χ_v in SI) of different iron minerals in saturated fine sands (10 $mg_{iron\ mineral}/g_{sand}$) show that the χ_v response of magnetite (87.90 SI) dominates the χ_v response of all the other minerals (χ_v ranges from 0.56 to 1.70 SI) (Figure 10a). Moreover, the χ_v of the equal proportions of magnetite + pyrite (79.34 SI), magnetite + hematite (88.32 SI), magnetite + goethite (81.80 SI), and magnetite + siderite (80.52 SI) as well as the mixture of equal proportions of all minerals together (89.18 SI) show insignificant changes in the χ_v response compared to χ_v response of magnetite alone (87.90 SI) (Figure 10b). The correlation between the χ_v response and different content (0–20 $mg_{iron\ mineral}/g_{sand}$) of magnetite shows a strong linear relationship ($y = 8.63x + 0.96$) with a correlation coefficient (R^2) equals 1 (Figure 10c). By changing the grain diameters of magnetite from 1.000–0.600 mm to 0.150–0.075 mm, the χ_v response shows a small change with an average value of 86.42 ± 1.39 SI (Figure 10d). At grain diameters of <0.075 mm, the χ_v response of magnetite decreases relatively to 70.01 (SI) (Figure 10d).

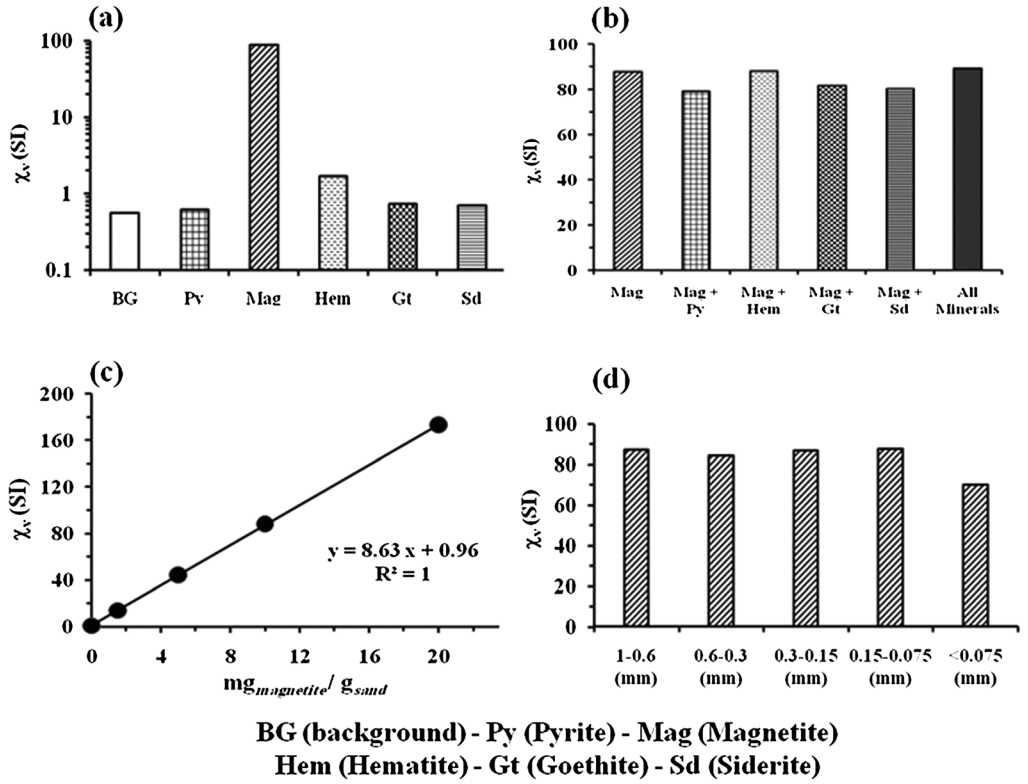

Figure 10. Volumetric magnetic susceptibility (χ_v) measurements in sands with (a) different iron minerals (10 $mg_{iron\ mineral}/g_{sand}$), (b) equal proportions of mixed iron minerals, (c) different content and fixed grain size (0.3–0.15 mm) of magnetite, and (d) different grain size and fixed content (10 $mg_{magnetite}/g_{sand}$) of magnetite. The χ_v response is dominated by magnetite mineral displaying a linear correlation with magnetite concentration and insignificant change with varying the grain size diameter of magnetite.

7. Discussion

7.1. Geophysical Signatures of Individual and Mixed Iron Phase Minerals

In a recent laboratory study investigating the spectral induced polarization responses of magnetite-Fe (II) redox reactions in porous media, *Hubbard et al*. [2014] hypothesized that under an applied electric field, the polarization response at the interface between the magnetite particle and the pore fluid is facilitated by the mobile charges within the magnetite particle, balanced by the buildup of oppositely charged ions in the pore fluid adjacent to the particle surface. This suggests that the electric double layer (EDL) and charge (ions) accumulation at the mineral fluid interface will be influenced by the number of mobile charge carriers (electrons and hole polarons) within the semiconductive iron minerals controlling the magnitude of the polarization response of the iron mineral. The same hypothesis can be applied to the magnitude of the electrochemical polarization associated with the redox reactions and charge transfer between the adsorbed electroactive ions and the iron mineral surface. In addition, the density of the charge carriers within the lattice structure of the iron mineral will contribute to the magnitude of the inphase component through the electronic conduction when grain to grain contact does exist. Accordingly, the variations in the population of charge carriers within the structure lattices of the iron mineral used in our study will most likely result in variation in the complex conductivity response.

Our results show that the magnitude of the complex conductivity parameters (inphase and quadrature conductivity) are in the order of pyrite > magnetite > hematite > goethite > siderite (Figure 4). We determined the density of mobile charge carriers (electrons or hole polarons) within the lattice structure of the iron minerals from the values of their band gaps (a gap between the valence band and conduction band where no electrons exist) [*Kingston and Neustadter*, 1955]. The lower the band gap, the higher the population of conduction electrons/hole polarons and hence the general electrical conductivity of the mineral [*Cornell and Schwertmann*, 2003]. The band gaps of the iron minerals used in our study and accordingly the density of

charge carriers within the minerals are in the order of magnetite (0.14 eV), pyrite (0.95 eV), hematite (2.2 eV), goethite (2.6 eV), and siderite (4.4 eV) [*Xu and Schoonen*, 2000; *Sherman*, 2009]. Based on the band gap values, there is relatively a good agreement between the density of charge carriers within the iron minerals and the complex conductivity response, except in the case of pyrite. Previous studies have documented that pyrite samples found in nature usually contain small amounts of other minor and trace elements (e.g., Cd, Ni, and As) that dramatically enhance the electrical properties of the mineral because they contain more free electrons or holes that can contribute to a large extent to the conductivity of the mineral [*Lehner et al*., 2006]. Due to the high band gap values and lower charge carriers within goethite and siderite minerals, they are classified as insulators and the conduction and polarization response of these iron minerals will be very low and closer to the response of the background sand. The small quadrature conductivity response of goethite, siderite, and hematite basically arises from ion migration within the electric double layer (EDL) at the mineral water interface [*Leroy et al*., 2008; *Vaudelet et al*., 2011a, 2011b; *Zhang et al*., 2012]. The conduction and polarization response of hematite is relatively higher than goethite and siderite due to the presence of few mobile charges within the structure lattices of hematite.

Both pyrite and magnetite show well-defined relaxation peaks in the quadrature conductivity spectra (σ'') centered at frequencies of 250 Hz and 1000 Hz, respectively (Figure 4a). These relaxation peaks are due to the strong EDL and electrochemical polarization of the interface between the iron mineral and pore fluid. The inphase conductivity response will be mostly controlled by the conductivity and volumetric content of the iron minerals, and the magnitude will follow the same order of the quadrature conductivity component (Figure 4b).

Our results show that the quadrature conductivity response of a porous medium containing mixed conductive (e.g., magnetite) and nonconductive (e.g., hematite, goethite, and siderite) iron minerals is dominated by the conductive mineral and is linearly proportional to its mass fraction (Figures 5a–5c). Accordingly, the presence of two conductive iron minerals (magnetite + pyrite) will increase the mass fractions of the polarized particles and therefore enhance the polarization response (Figure 3d). Most interestingly, we observed that the relaxation peak of the magnetite-pyrite-sand mixture is dominated by the pyrite which can be explained by the relatively higher polarizability of pyrite compared to magnetite. The inphase response of the conductive (e.g., magnetite) and nonconductive (e.g., hematite, goethite and siderite) iron mineral-sand mixture was observed to be lower in magnitude than the response of the individual iron minerals (Figures 6a–6b). The contribution of electronic conduction of the conductive iron minerals to the measured inphase response requires a grain to grain contact of the conductive iron mineral resulting in a continuous electronic conduction path. The presence of nonconductive iron minerals will break down such a connection and mask the contribution of electronic conduction of the conductive iron mineral. However, the presence of two different conductive iron minerals in the sand (magnetite + pyrite) enhances the magnitude of the inphase response compared to the individual response of each mineral (Figure 6d). The enhancement in the inphase response results from the increase in grain to grain contacts of the conductive minerals and the resulting electronic conduction path between the two conductive iron minerals.

The magnetic susceptibility measurements are highly dominated by magnetite, which is 86 times higher than the other measured iron minerals. Magnetite is a spinel group mixed ferrous-ferric iron oxide mineral with ferrimagnetic properties. In magnetite, two thirds of the iron atoms align themselves in one direction, but the remaining one third of the iron atoms are aligned in the opposite direction [*Mullins*, 1977; *Dearing et al*., 1985]. This results in a strong positively aligned magnetic moment when placed in an appropriate field [*Mullins*, 1977; *Dearing et al*., 1985]. Pyrite and siderite are paramagnetic minerals, whereas hematite and goethite are antiferromagnetic minerals and all are known to have very small magnetic susceptibilities. Therefore, the presence of magnetite in porous media will dominate the magnetic susceptibility response even if trace amounts are present [*Dearing et al*., 1985]. This is supported by our results where equal proportions of iron minerals are mixed and the magnetic susceptibility response was approximately equal to the response of magnetite alone (Figure 10).

Figure 11 shows a cross plot of the quadrature conductivity at 100 Hz and magnetic susceptibility measurements of the iron minerals samples (10 $mg_{iron\ mineral}/g_{sand}$ and 0.3–0.15 mm grain diameter) used in this study. The plot displays three different types of geophysical signatures as follows: type (I) representing magnetite showing high quadrature conductivity (σ'') and magnetic susceptibility (χ_v), type (II) representing pyrite showing high quadrature conductivity and low magnetic susceptibility, and type (III)

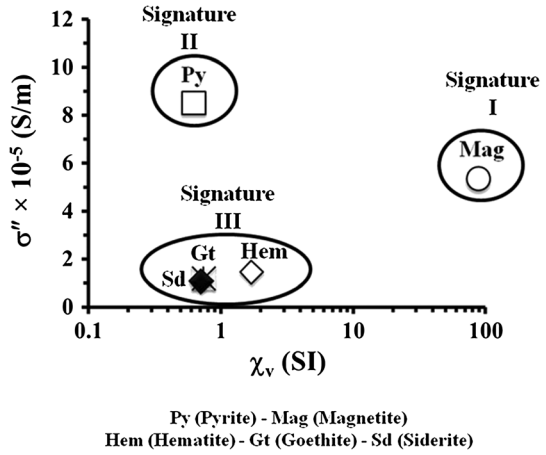

Figure 11. Cross plot of quadrature conductivity (σ'') at 100 Hz versus magnetic susceptibility (χ_v) of iron minerals (10 $mg_{iron\ mineral}/g_{sand}$ and 0.3–0.15 mm grain diameter) disseminated in saturated fine sand. Three different types of geophysical signatures are observed as follow: type (I) representing magnetite showing high σ'' and χ_v, type (II) representing pyrite showing high σ'' and low χ_v, and type (III) representing hematite, goethite, and siderite, showing low σ'' and χ_v.

representing hematite, goethite, and siderite, showing low quadrature conductivity and low magnetic susceptibility. The cross plot clearly demonstrates the advantage of integrating the complex conductivity and magnetic susceptibility methods and the joint interpretation of the obtained results.

7.2. Geophysical Signatures of Different Iron Mineral Content and Grain Size

Under different redox conditions, the interaction between microorganisms and minerals at low temperatures often lead to acceleration and transformation of iron mineral phases through dissolution and precipitation. The dissolution and precipitation processes will decrease or increase the mass/volumetric content as well as surface area of iron minerals [*Schwertmann and Fitzpatrick*, 1992]. Relationships between the magnitude of the IP effect and the percentages of metallic minerals are well documented [*Pelton et al*., 1978; *Vanhala and Peltoniemi*, 1992; *Seigel et al*., 1997; *Bigalke and Junge*, 1999]. Under the same grain size diameter of the iron minerals, our results show that the increase in polarized particles of pyrite or magnetite content increases the quadrature conductivity magnitude with a strong power law relationship ($R^2 > 0.95$). The similar power law exponents of pyrite (0.68) and magnetite (0.64) indicate that the polarization mechanisms for the two iron minerals are similar; however, the magnitude is higher in the case of the highly polarized pyrite. The increase in the content of pyrite and magnetite increases the grain to grain contacts of the conductive minerals resulting in a relatively high enhancement in the electronic conduction path and the inphase magnitudes. The strong power law equations for the quadrature conductivity component (Figure 7c) can be used to estimate the content of the pyrite or magnetite in the subsurface porous media. In addition, a strong linear relationship was obtained between the magnetite content and magnetic susceptibility (Figure 11b) which can be used to estimate the magnetite content from the magnetic susceptibility measurements. Our results show that the increase in pyrite content will significantly increase the magnitude of the quadrature conductivity component, whereas the increase in magnetite content will significantly increase both the quadrature conductivity and magnetic susceptibility magnitudes. These distinctive observations can be used to discriminate between the two iron minerals using integrated complex conductivity and magnetic susceptibility measurements.

Under the same mass fraction, the decrease in iron mineral grain size in sediments will enhance the surface area of the polarized iron mineral particles and increase the polarization magnitude. Previous studies showed that the characteristic relaxation time constant of metals in sediments was experimentally found to be proportional to the square of the grain size of the metallic minerals [*Pelton et al*., 1978; *Wong*, 1979; *Wait*, 1982; *Olhoeft*, 1985; *Slater et al*., 2005]. Our results clearly demonstrate that under the same iron mineral content, there is a progressive increase in quadrature conductivity magnitude and shift in the relaxation peaks to higher frequencies with decreasing grain size diameters of pyrite and magnetite particles (Figure 8). However, the magnitude of the quadrature conductivity and the frequency values of the characteristic relaxation peaks were lower in magnetite compared to pyrite due to the relatively higher polarizability of pyrite.

Despite the fact that most of the biogenic iron minerals are in the nanometer scale (2–500 nm) [*Fortin and Châtellier*, 2003], our main intention here is to demonstrate the effect of grain size diameters of iron mineral particles on the complex conductivity response. According to our results, one should expect that the relaxation peak of the polarization response of the nanoparticulate iron biominerals will be observed at very high frequencies (>1 KHz) not attainable with the field complex conductivity instruments. While this is true,

our results still show a difference in the magnitude of the polarization response at frequencies (<100 Hz) below the frequencies of the relaxation peaks which can be used to discriminate between the different grain size of the iron minerals. Moreover, we expect that the progressive nucleation and crystal growth of iron minerals as well as the possible aggregation of the produced nanoparticulate and adsorption to the nonmetallic grains of the porous material will exhibit a similar effect as demonstrated for the grain size range of our results. This is supported by the study of *Atekwana et al*. [2014] where scanning electron microscopy images (see Figures 9a and 9c) show magnetite coating sand grains (millimeter scale) within the zone of enhanced complex conductivity response observed by *Mewafy et al*. [2013]. Also, the study by *Slater et al*. [2007] explained the polarization response associated with sulfide biomineralization under anaerobic conditions due to the biomineral encrusted pores. The study by *Joyce et al*. [2012] using spectral-induced polarization (complex conductivity) measurements of different nonmetallic particles showed that both nanosilver and nanozero valent iron displayed a relaxation peak at 50 Hz and 500 Hz, respectively. The author related the low-frequency-dependent response to the formation of aggregates that increased the particle size to microsized particles. Moreover, we expect that the magnitude of the complex conductivity response of the nanoparticulate iron mineral will be higher due to the high-surface reactivity of these minerals which will be highly detectable and discriminable at lower frequencies. Moreover, the latest development in field instrumentation is attempting to expand the frequency range that can be measured in the field.

For a simple case of porous media containing only one grain size of pyrite or magnetite, the obtained power law relationship between the quadrature conductivity and grain size diameters of pyrite and magnetite can be used to estimate the grain size diameters of the iron minerals (Figure 8c). For a complex system with two different grain sizes of iron minerals, the results clearly demonstrate that the polarization and conduction mechanisms of the mixture (e.g., pyrite) are additive (Figure 9). On the other hand, the variations in the grain size diameters of magnetite particles showed very minimal effect on the measured magnetic susceptibility (Figure 11c). This is because the magnetite will show only a multidomain magnetic susceptibility response for the range of grain size diameters used in this experiment [*Dearing et al*., 1996]. The grain size of biogenic iron minerals are mostly in the nanometer scale which will exhibit a single-domain or superparamagnetic response [*Dearing et al*., 1996]. Therefore, a wide range of grain size diameters (nanomillimeters) is required to induce a change in the measured magnetic susceptibility. The concentration or content of the magnetite mineral is more important than the variations in grain size diameters as supported by our observations. Therefore, the variations in grain size diameters of biogenic iron minerals will be highly detectable using complex conductivity measurements, whereas the variation in content will be highly detectable by both complex conductivity and magnetic susceptibility.

7.3. Implications

Here we provide a schematic diagram summarizing the main findings of the present study (Figure 12) and then provide an example for how these findings can be used to investigate some of the biophysicochemical processes in the subsurface environment (Figure 13). Figure 10a shows that the microbial mineral interactions and associated biophysicochemical processes (e.g., iron or sulfate reduction) may enhance the production of Fe(II) in solution which will react with Fe (III), HS^-, and $HCO3^-$ and form different iron phase minerals. These iron minerals display different complex conductivity and magnetic susceptibility signatures. Both pyrite and magnetite display the highest complex conductivity response, and only magnetite shows the highest magnetic susceptibility response. The hematite, goethite, and siderite iron minerals display low complex conductivity and magnetic susceptibility response and are found to be undetectable under our experimental conditions using these two different techniques. In the case where the biophysicochemical process results in a mixture of two different iron minerals (Figure 12b), the complex conductivity and magnetic susceptibility response will be dominated by the most conductive and magnetic iron mineral, respectively. Figure 12c shows that both the quadrature conductivity and magnetic susceptibility were sensitive to the iron mineral content (e.g., magnetite) exhibiting a strong power law and linear relationship, respectively. Iron mineral dissolution and precipitation resulting in different grain size diameters will impact the complex conductivity response by increasing the magnitude of the quadrature conductivity and shifting the relaxation peak to higher frequencies with decreasing grain size diameter (Figure 12d). The mixture of two different grain sizes for the same iron mineral will display an average quadrature conductivity response (Figure 12d). The magnetic susceptibility measurements were insensitive to the grain size ranges used in our study (Figure 12d).

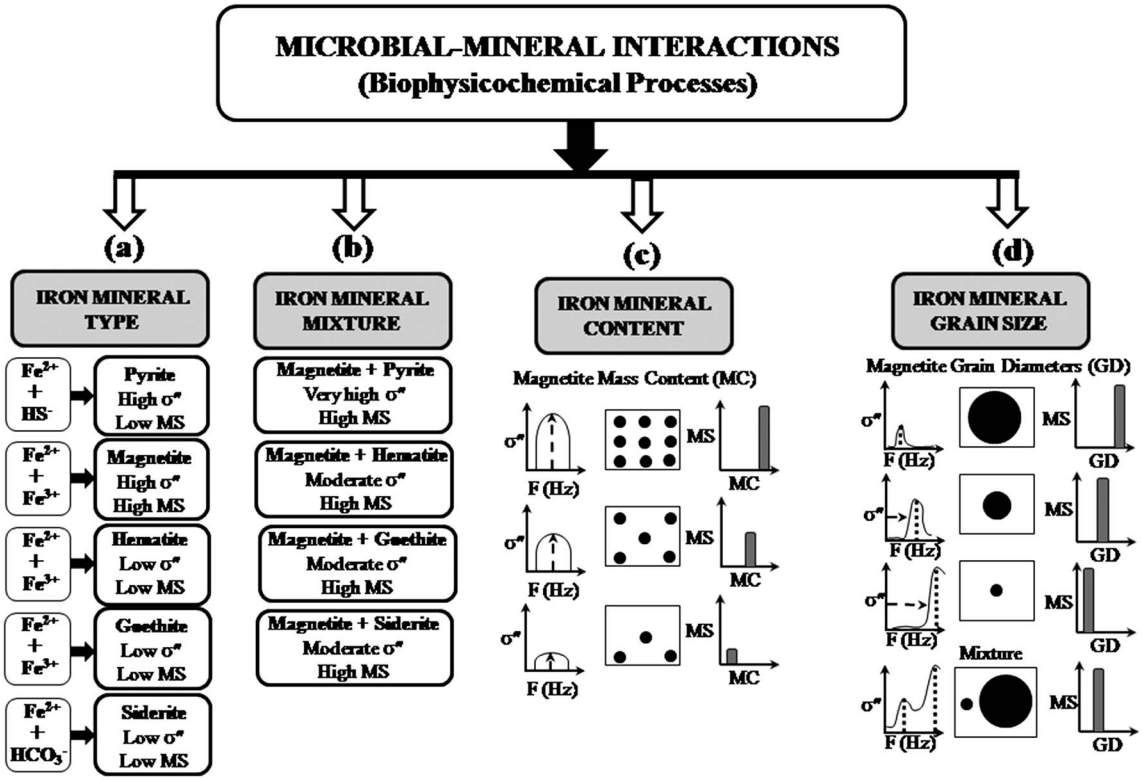

Figure 12. Schematic diagram summarizing under our experimental conditions the quadrature conductivity (σ'') and magnetic susceptibility (MS) signatures of (a) different iron minerals, (b) iron minerals mixtures, (c) iron mineral content, and (d) individual iron mineral grain size and mixtures resulting from the biophysicochemical processes associated with the microbial mineral interactions.

Under our laboratory experimental conditions, the characteristic complex conductivity and magnetic susceptibility properties of the measured iron mineral phases can be used to discriminate between these minerals and infer some information about the subsurface biophysicochemical conditions associated with the microbial mineral interactions. In a review article of anaerobic oxidation of methane (AOM), *Caldwell et al.* [2008] proposed that the sulfate-methane transition (SMT) zone in marine sediments which is created and

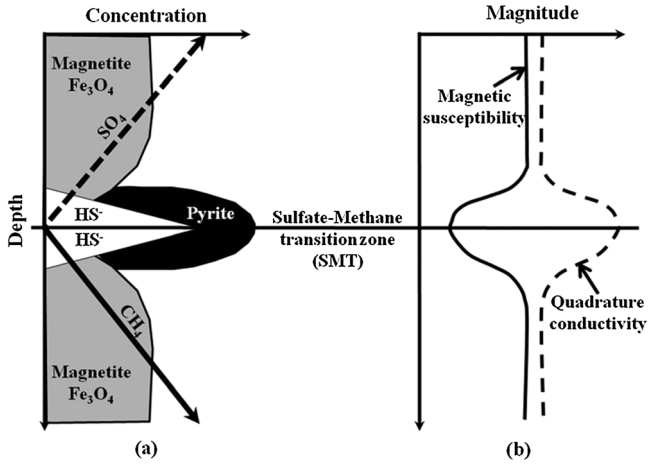

Figure 13. Schematic diagram showing how the integration of quadrature conductivity (σ'') and magnetic susceptibility (MS) measurements can be used to precisely map the sulfate-methane transition (SMT) zone in marine sediments where the anaerobic oxidation of methane (AOM) is coupled to the sulfate reduction. (a) The SMT zone is characterized by depletion in iron oxides minerals (e.g., magnetite) which are biotransformed to pyrite resulting in (b) a decrease in the magnetic susceptibility magnitude and increase in the quadrature conductivity (σ'') magnitude.

maintained by AOM consortia may be studied with geophysical tools. These biogeophysical tools provide rapid determination of AOM activity due to the sensitivity of these techniques to the presence of microbially induced mineralization of magnetic or nonmagnetic iron sulfides left by AOM communities. Figure 13a shows the biophysicochemical processes within the SMT zone which can be summarized from the study of *Riedinger et al*. [2005] by the following reactions:

$$CH_4 + SO_4^{2-} \rightarrow HCO_3^- + H_2O + HS^-, \quad (4)$$

$$Fe_3O_4 + HS^- + 7H^+ \rightarrow 3Fe^{2+} + S^o + 4H_2O, \quad (5)$$

$$Fe^{2+} + HS^- \rightarrow FeS_s + H^+, \quad (6)$$

$$FeS_{(s)} + HS^-_{(aq)} + H^+_{(aq)} \rightarrow FeS_{2(s)} + H_{2(g)}. \quad (7)$$

Equation (4) represents the coupling of sulfate reduction and anaerobic oxidation of methane resulting in the enrichment of HS^- within the coupling interface. Equation (5) shows that the production of HS^- facilitates the reduction of iron oxides such as magnetite resulting in a production of Fe^{2+} which will react with HS^- (equation (6)) producing iron monosulfide (FeS) solid phase. The FeS is unstable and will be converted immediately to pyrite by further interaction with HS^- (equation (7)). The net result of such biogeochemical process is depletion in the iron oxide mineral represented here by magnetite at the SMT zone with the enrichment of pyrite. Previous studies showed that the SMT zone is characterized by distinct minima in magnetic susceptibility due to the conversion of initial magnetic minerals to pyrite (pyritization) [*Garming et al*., 2005; *Riedinger et al*., 2005]. Our results show that pyrite is less magnetic and highly polarizable. Therefore, the SMT zone will be characterized by minima in the magnetic susceptibility versus depth distribution (due to depletion of magnetite) and maxima in the quadrature conductivity (due to enrichment with highly polarizable pyrite grains) as demonstrated in Figure 13b. Therefore, we postulate, based on our laboratory work, that the SMT zone can be precisely mapped by integrating complex conductivity and magnetic susceptibility measurements reducing the need for extensive coring and analyses of pore water sulfate and methane concentration.

8. Conclusions

The present study demonstrates the advantage of integrating complex conductivity (in particular the quadrature conductivity component) and magnetic susceptibility measurements to discriminate between different iron minerals under variable conditions. Pyrite and magnetite were the highly polarized and conductive minerals compared to hematite, goethite, and siderite, whereas magnetite is the only highly magnetic mineral and the presence of a small percentage of magnetite will dominate the magnetic susceptibility measurements of all these minerals together. The high interfacial polarizability of pyrite and magnetite are due to the high population of conduction electrons within the structure lattices of the minerals contributing indirectly to the polarization of the electric double layer and directly to the electrochemical polarization due to charge transfer between adsorbed redox electroactive species and iron mineral surface.

The quadrature conductivity is shown to be more sensitive than magnetic susceptibility to the variations in grain size diameters (showing additive response) of iron minerals (e.g., pyrite and magnetite). Strong power law relationships were established from quadrature conductivity and magnetic susceptibility measurements that can be used to quantitatively estimate the mass fraction of highly polarized (e.g., pyrite and magnetite) and magnetic (e.g., magnetite) iron minerals, respectively.

The results of our study may have implications for the successful investigations of microbial mineral interactions and biophysicochemical processes resulting in biotransformation or precipitation of secondary iron mineral phases with different electrical and magnetic properties. For example, integrating complex conductivity and magnetic susceptibility may be useful in (1) locating the sulfate-methane transition (SMT) zone due to the presence of iron sulfides, (2) monitoring the biogeochemical conversion of initial magnetic minerals to pyrite (pyritization) due to the sulfate reduction coupled to the anaerobic oxidation of methane (AOM) and (3) monitoring bioremediation strategies that result in the precipitation of mineral phases with different electrical and magnetic prosperities.

Acknowledgments
This work is funded by the U.S. Department of Energy (award DE-SC0007118) and Chevron Energy Technology Company (grant CW852844). This is the Boone Pickens School of Geology contribution 2014-14.

References

Atekwana, E. A., F. M. Mewafy, G. Abdel Aal, D. D. Werkema Jr., A. Revil, and L. D. Slater (2014), High-resolution magnetic susceptibility measurements for investigating magnetic mineral formation during microbial mediated iron reduction, *J. Geophys. Res. Biogeosci.*, *119*, 80–94, doi:10.1002/2013JG002414.

Bazylinski, D. A., and R. B. Frankel (2003), Biologically controlled mineralization in prokaryotes, *Rev. Mineral. Geochem.*, *54*, 217–247.

Bigalke, J., and A. Junge (1999), Using evidence of non-linear induced polarization for detecting extended ore mineralizations, *Geophys. J. Int.*, *137*, 516–520.

Blöthe, M., and E. E. Roden (2009), Microbial iron redox cycling in a circumneutral pH groundwater seep, *Appl. Environ. Microbiol.*, *75*, 468–473.

Caldwell, S. L., J. R. Laidler, E. A. Brewer, J. O. Eberly, S. C. Sandborgh, and F. S. Colwell (2008), Anaerobic oxidation of methane: Mechanisms, biogenetics, and the ecology of associated microorganisms, *Environ. Sci. Technol.*, *42*(18), 6791–6799.

Cooper, D., F. Picardal, and A. Coby (2006), Interactions between microbial iron reduction and metal geochemistry: Effect of redox cycling on transition metal speciation in iron bearing sediments, *Environ. Sci. Technol.*, *40*, 1884–1891.

Cornell, R. M., and U. Schwertmann (2003), *The Iron Oxides: Structure, Properties, Reactions, Occurrences and Uses*, 664 pp., WILEY-VCH Verlag GmbH & Co. KGaA, Weinheim, Germany.

Dearing, J. A., B. A. Maher, and F. Oldfield (1985), Geomorphological linkages between soils and sediments: The role of magnetic measurements, in *Geomorphology and Soils*, edited by K. S. Richards, R. R. Arnett, and S. K. Ellis, 441 pp., George Allen and Wnwin, London, U. K.

Dearing, J. A., R. J. L. Dann, K. Hay, J. A. Lees, P. J. Loveland, B. A. Maher, and K. O'Grady (1996), Frequency-dependent susceptibility measurements of environmental materials, *Geophys. J. Int.*, *124*, 228–240.

Dukhin, S. S., and V. N. Shilov (2002), Non-equilibrium electric surface phenomena and extended electrokinetic characterization of particles, in *Interfacial Electrokinetics and Electrophoresis*, *Surfactant Sci. Ser.*, vol. 106, edited by A. V. Delgado, pp. 55–85, Marcel Dekker, New York.

Flores Orozco, A., K. H. Williams, P. E. Long, S. S. Hubbard, and A. Kemna (2011), Using complex resistivity imaging to infer biogeochemical processes associated with bioremediation of an uranium contaminated aquifer, *J. Geophys. Res.*, *116*, G03001, doi:10.1029/2010JG001591.

Fortin, D., and X. Châtellier (2003), Biogenic iron oxides, in *Recent Research Developments in Mineralogy*, vol. 3, edited by S. G. Pandalai, pp. 47–63, Research Signpost, Trivandrum, Kerala, India.

Fredrickson, J. K., J. M. Zachara, D. W. Kennedy, H. Dong, T. C. Onstott, N. W. Hinman, and S. M. Li (1998), Biogenic iron mineralization accompanying the dissimilatory reduction of hydrous ferric oxide by a groundwater bacterium, *Geochim. Cosmochim. Acta*, *62*, 3239–3257.

Garming, J. F. L., U. Bleil, and N. Riedinger (2005), Alteration of magnetic mineralogy at the sulfate–methane transition: Analysis of sediments from the Argentine continental slope, *Phys. Earth Planet. Inter.*, *151*, 290–308.

Gurin, G., A. Tarasov, Y. Ilyin, and K. Titov (2013), Time domain spectral induced polarization of disseminated electronic conductors: Laboratory data analysis through the Debye decomposition approach, *J. Appl. Geophys.*, *98*, 44–53.

Hubbard, C. G., L. J. West, J. D. Rodriguez-Blanco, and S. Shaw (2014), Laboratory study of spectral induced polarization responses of magnetite—Fe^{2+} redox reactions in porous media, *Geophysics*, *79*(1), D21–D30.

Joyce, R. A., D. R. Glasser, D. D. WerkemaJr, and E. A. Atekwana (2012), Spectral induced polarization response to nanoparticles in a saturated sand matrix, *J. Appl. Geophys.*, *77*, 63–71.

Kappler, A., and K. L. Straub (2005), Geomicrobiological cycling of iron, in *Molecular Geomicrobiology*, vol. 59, edited by J. F. Banfield, J. Cervini-Silva, and K. H. Nealson, pp. 85–108, The Mineralogical Society of America, Chantilly, Va.

Kingston, R. H., and S. F. Neustadter (1955), Calculation of the space charge, electric field, and free carrier concentration at the surface of a semiconductor, *J. Appl. Phys.*, *26*, 718–720.

Klueglein, N., T. Lsekann-Behrens, M. Obst, S. Behrens, E. Appel, and A. Kappler (2013), Magnetite formation by the novel Fe(III)-reducing geothrix fermentans strain HradG1 isolated from a hydrocarbon-contaminated sediment with increased magnetic susceptibility, *Geomicrobiol. J.*, *30*(10), 863–873, doi:10.1080/01490451.2013.790922.

Lehner, S. W., K. S. Savage, and J. C. Ayers (2006), Vapor growth and characterization of pyrite (FeS_2) doped with Co, Ni, and As: Variation in semiconducting properties, *J. Cryst. Growth*, *286*, 306–317.

Leroy, P., A. Revil, A. Kemna, P. Cosenza, and A. Ghorbani (2008), Complex conductivity of water saturated packs of glass beads, *J. Colloid Interface Sci.*, *321*(1), 103−117.

Lesmes, D. P., and K. M. Frye (2001), Influence of pore fluid chemistry on the complex conductivity and induced polarization responses of Berea sandstone, *J. Geophys. Res.*, *106*(B3), 4079–4090, doi:10.1029/2000JB900392.

Liu, S. V., J. Zhou, C. Zhang, D. R. Cole, P. Gajdarziska-Josifovska, and T. J. Phelps (1997), Thermophilic Fe(III)-reducing bacteria from the deep subsurface: The evolutionary implications, *Science*, *277*, 1106–1109.

Lovley, D. R. (1991), Dissimilatory Fe(III) and Mn(IV) reduction, *Microbiol. Rev.*, *55*, 259–287.

Lovley, D. R. (1993), Dissimilatory metal reduction, *Annu. Rev. Microbiol.*, *47*, 263–290.

Lowenstam, H. A. (1986), Mineralization processes in monerans and protoctists, in *Biomineralization in Lower Plants and Animals*, vol. 30, edited by B. S. C. Leadbeater and R. Riding, pp. 1–17, Oxford Univ. Press, New York.

Mansoor, N., and L. Slater (2007), On the relationship between iron concentration and induced polarization in marsh soils, *Geophysics*, *72*(1), A1–A5.

Marcon, P., K. Bartusek, M. Budrkova, and Z. Dokoupil (2011), Magnetic susceptibility measurement using 2D magnetic resonance imaging, *Meas. Sci. Technol.*, *22*, 105,702, doi:10.1088/0957-0233/22/10/105702.

Mewafy, F. M., E. A. Atekwana, D. D. Werkema Jr., L. D. Slater, D. Ntarlagiannis, A. Revil, M. Skold, and G. N. Delin (2011), Magnetic susceptibility as a proxy for investigating microbially mediated iron reduction, *Geophys. Res. Lett.*, *38*, L21402, doi:10.1029/2011GL049271.

Mewafy, F. M., D. D. Werkema, E. A. Atekwana, L. D. Slater, G. Z. Abdel Aal, A. Revil, and D. Ntarlagiannis (2013), Evidence that bio-metallic mineral precipitation enhances the complex conductivity response at a hydrocarbon contaminated site, *J. Appl. Geophys.*, *98*, 113–123.

Mullins, C. E. (1977), Magnetic susceptibility of the soil and its significance in soil science—A review, *J. Soil Sci.*, *28*, 223–246.

Nealson, K. H., and D. Saffarini (1994), Iron and manganese in anaerobic respiration: Environmental significance, physiology, and regulation, *Annu. Rev. Microbiol.*, *48*, 311–343.

Ntarlagiannis, D., K. H. Williams, L. Slater, and S. Hubbard (2005), Low frequency electrical response to microbial induced sulfide precipitation, *J. Geophys. Res.*, *110*, G02009, doi:10.1029/2005JG0000.

Ntarlagiannis, D., R. Doherty, and K. H. Williams (2010), Spectral induced polarization signatures of abiotic FeS precipitation, *Geophysics*, *75*(4), F127–F133.

Olhoeft, G. R. (1985), Low-frequency electrical properties, *Geophysics*, *50*, 2492–2503.

Pelton, W. H., S. H. Ward, P. G. Hallof, W. R. Sill, and P. H. Nelson (1978), Mineral discrimination and removal of inductive coupling with multifrequency IP, *Geophysics*, *43*, 588–609.

Personna, Y. R., D. Ntarlagiannis, L. Slater, N. Yee, M. O'Brien, and S. Hubbard (2008), Spectral induced polarization and electrodic potential monitoring of microbially mediated iron sulfide transformation, *J. Geophys. Res.*, *113*, G02020, doi:10.1029/2007JG000614.
Porsch, K., M. L. Rijal, T. Borch, L. D. Troyer, S. Behrens, F. Wehland, E. Appel, and A. Kappler (2013), Impact of organic carbon and iron bioavailability on the magnetic susceptibility of soils, *Geochim. Cosmochim. Acta*, *128*, 44–57, doi:10.1016/j.gca.2013.12.001.
Postma, D. (1981), Formation of siderite and vivianite and the pore-water composition of a recent bog sediment in Denmark, *Chem. Geol.*, *31*, 225–244.
Revil, A., and P. W. J. Glover (1998), Nature of surface electrical conductivity in natural sands, sandstones, and clays, *J. Geophys. Res.*, *25*, 691–694, doi:10.1029/98GL00296.
Revil, A., M. Karaoulis, T. Johnson, and A. Kemna (2012a), Review: Some low-frequency electrical methods for subsurface characterization and monitoring in hydrogeology, *Hydrogeol. J.*, *20*(4), 617–658, doi:10.1007/s10040-011-0819-x.
Revil, A., E. Atekwana, C. Zhang, A. Jardani, and S. Smith (2012b), A new model for the spectral induced polarization signature of bacterial growth in porous media, *Water Resour. Res.*, *48*, W09545, doi:10.1029/2012WR011965.
Revil, A., M. Karaoulis, S. Srivastava, and S. Byrdina (2013), Thermoelectric self-potential and resistivity data localize the burning front of underground coal fires, *Geophysics*, *78*(5), B259–B273.
Riedinger, N., K. Pfeifer, S. Kasten, J. F. L. Garming, C. Vogt, and C. Hensen (2005), Diagenetic alteration of magnetic signals by anaerobic oxidation of methane related to a change in sedimentation rate, *Geochim. Cosmochim. Acta*, *69*(16), 4117–4126.
Rijal, M. L., E. Appel, E. Petrovsky, and U. Blaha (2010), Change of magnetic properties due to fluctuations of hydrocarbon contaminated groundwater in unconsolidated sediments, *Environ. Pollut.*, *158*(5), 1756–1762.
Rijal, M. L., K. Porsch, E. Appel, and A. Kappler (2012), Magnetic signature of hydrocarbon-contaminated soils and sediments at the former oil field Hänigsen, Germany, *Stud. Geophys. Geod.*, *56*(3), 889–908.
Roden, E. E., and J. M. Zachara (1996), Microbial reduction of crystalline iron (III) oxides: Influence of oxide surfaces area and potential for cell growth, *Environ. Sci. Technol.*, *30*, 1618–1628.
Roh, Y., R. J. Lauf, A. D. McMillan, C. Zhang, C. J. Rawn, J. Bai, and T. J. Phelps (2001), Microbial synthesis and the characterization of some metal-doped magnetite, *Solid State Commun.*, *118*, 529–534.
Schön, J. H. (1996), *Physical Properties of Rocks: Fundamentals and Principles of Petrophysics, Handbook of Geophysical Exploration: Seismic Exploration*, vol. 18, 583 pp., Pergamon, New York.
Schwertmann, U., and R. W. Fitzpatrick (1992), Iron minerals in surface environments, in *Biomineralization Processes of Iron and Manganese—Modem and Ancient Environments*, Catena Suppl., vol. 21, edited by H. C. W. Skinner and R. W. Fitzpatrick, pp. 7–30, Cremlingen-Destedt, Catena Verlag.
Seigel, H. O., H. Vanhala, and S. Nicholas Sheard (1997), Some case histories of source discrimination using time-domain spectral IP, *Geophysics*, *62*, 1394–1408.
Sherman, D. M. (2009), Electronic structures of siderite ($FeCO_3$) and rhodochrosite ($MnCO_3$): Oxygen K-edge spectroscopy and hybrid density functional theory, *Am. Mineral.*, *94*, 166–171.
Slater, L. (2007), Near surface electrical characterization of hydraulic conductivity: From petrophysical properties to aquifer geometries—A review, *Surv. Geophys.*, *28*, 169–197.
Slater, L. D., J. Choi, and Y. Wu (2005), Electrical properties of iron-sand columns: Implications for induced polarization investigation and performance monitoring of iron-wall barriers, *Geophysics*, *70*(4), G87–G94.
Slater, L., D. Ntarlagiannis, and D. Wishart (2006), On the relationship between induced polarization and surface area in metal-sand and clay-sand mixtures, *Geophysics*, *71*(2), A1–A5.
Slater, L., D. Ntarlagiannis, Y. R. Personna, and S. Hubbard (2007), Pore-scale spectral induced polarization signatures associated with FeS biomineral transformations, *Geophys. Res. Lett.*, *34*, L21404, doi:10.1029/2007GL031840.
Vanhala, H., and M. Peltoniemi (1992), Spectral IP studies of Finnish ore prospects, *Geophysics*, *57*, 1545–1555.
Vaudelet, P., A. Revil, M. Schmutz, M. Franceschi, and P. Bégassat (2011a), Changes in induced polarization associated with the sorption of sodium, lead, and zinc on silica sands, *J. Colloid Interface Sci.*, *360*, 739–752.
Vaudelet, P., A. Revil, M. Schmutz, M. Franceschi, and P. Bégassat (2011b), Induced polarization signature of the presence of copper in saturated sands, *Water Resour. Res.*, *47*, W02526, doi:10.1029/2010WR009310.
Vinegar, H. J., and M. H. Waxman (1984), Induced polarization of shaly sands, *Geophysics*, *49*(8), 1267–1287.
Wait, J. R. (1982), *Geo-Electromagnetism*, Academic Press Inc., New York.
Waxman, M. H., and L. J. M. Smits (1968), Electrical conductivities in oil-bearing shaly sands, *Soc. Pet. Eng. J.*, *8*(2), 107–122.
Williams, K. H., D. Ntarlagiannis, L. D. Slater, A. Dohnalkova, S. S. Hubbard, and J. F. Banfield (2005), Geophysical imaging of stimulated microbial biomineralization, *Environ. Sci. Technol.*, *39*, 7592–7600.
Williams, K. H., A. Kenya, M. J. Wilkins, J. Druhan, E. Arntzen, A. L. N'Guessan, P. E. Long, S. S. Hubbard, and J. F. Banfield (2009), Geophysical monitoring of coupled microbial and geochemical processes during stimulated subsurface bioremediation, *Environ. Sci. Technol.*, *43*, 6717–6723.
Wong, J. (1979), An electrochemical model of the induced polarization phenomenon in disseminated sulfide ores, *Geophysics*, *44*, 1245–1265.
Wu, Y., L. D. Slater, and N. Korte (2005), Effect of precipitation on low frequency electrical properties of zero valent iron columns, *Environ. Sci. Technol.*, *39*, 9197–9204.
Wu, Y., L. D. Slater, R. Versteeg, and D. LaBrecque (2009), Calcite precipitation dominates the electrical signatures of zero valent iron column under simulated field conditions, *J. Contam. Hydrol.*, *106*, 131–143.
Xu, Y., and M. A. A. Schoonen (2000), The absolute energy positions of conduction and valence bands of selected semiconducting minerals, *Am. Mineral.*, *85*, 543–556.
Zhang, C., S. Liu, T. J. Phelps, D. R. Cole, J. Horita, S. M. Fortier, M. Elless, and J. W. Valley (1997), Physiochemical, mineralogical, and isotopic characterization of magnetite rich iron oxides formed by thermophilic bacteria, *Geochim. Cosmochim. Acta*, *61*, 4621–4632.
Zhang, C., H. Vali, C. S. Romanek, T. J. Phelps, and S. Liu (1998), Formation of single-domain magnetite by a thermophilic bacterium, *Am. Mineral.*, *83*, 1409–1418.
Zhang, C., L. Slater, G. Redden, Y. Fujita, T. Johnson, and D. Fo (2012), Spectral induced polarization signatures of hydroxide adsorption and mineral precipitation in porous media, *Environ. Sci. Technol.*, *46*, 4357–4364.